Supporting Information

Design of Water-soluble CdS-Titanate-Nickel Nanocomposites for Photocatalytic Hydrogen Production under sunlight

Cao-Thang Dinh,[†] Minh-Hao Pham,[†] Freddy Kleitz,[§] and Trong-On Do*[†]

[†] Department of Chemical Engineering and Centre de Catalyse et Chimie Verte (C3V), Laval University, Quebec, G1V 0A6, Canada

[§] Department of Chemistry and Centre de Recherche sur les Matériaux Avancés (CERMA), Laval University, Quebec, G1V 0A6, Canada

Corresponding Author : trong-on.do@gch.ulaval.ca

Chemicals. All chemicals were used as received; Titanium butoxide (TB), benzyl alcohol (BA), oleylamine (OM), benzyl ether, tetraethylammonium (TEA) hydroxide, nickel nitrate, cadmium nitrate, thiourea, chloroplatinic acid, were purchased form Aldrich. Absolute ethanol, acetone, and toluene solvents were of analytical grade and were also purchased form Aldrich.

Synthesis of titanate nanodisks. In a typical synthesis, 2g of TB, 12 g of OM, 12g of BA (OM:BA weight ratio of 1:1), and 30g of benzyl ether were added to a 100-mL round-bottom flask. The reaction mixture was heated to 190 ^{o}C at the heating rate 5 ^{o}C/min under nitrogen flow. After 20 h, the reaction was stopped and cooled down to room temperature. After addition of excess absolute ethanol, the TNDs were obtained by centrifugation. The obtained nanodisks were then re-dispersed in toluene and re-precipitated with ethanol. This process was repeated three times to remove the un-reacted reagents.

Tetraethylammonium-exchanged titanate nanodisks. The as-synthesized TNDs were treated with tetraethylammonium hydroxide to obtain water-soluble TEA-TNDs. Typically, 5 mmol of as-synthesized TNDs (according to Ti atom) were dispersed in a mixture of TEAOH (15 mmol), ethanol (15 ml) and water (15 ml). The mixture was stirred overnight at room temperature. An excess of acetone was added to the obtained clear solution to precipitate TNDs. The precipitate was then washed several times with acetone and finally re-dispersed in 10 ml of water.

Synthesis of CdS-TND hybrids. The CdS-TND hybrids were synthesized using a multi-cycle pathway (Figure 1). In the first cycle, Cd^{2+} cations-exchanged TNDs were prepared. Accordingly, the TEA-TNDs dispersed in water were gradually added to a solution containing Cd^{2+} cations (Cd:Ti atomic ratio of 1:2) under stirring. The resulting Cd^{2+}-TND precipitate was then washed several times with water to remove un-exchanged Cd^{2+} cations. To obtain the CdS-TND hybrid, Cd^{2+}-TNDs was then dispersed in water. To this mixture was added a solution containing both TEAOH and thiourea (TEAOH : thiourea : Cd^{2+} molar ratio of 1:1:0.3). Next, the obtained mixture was heated to 70^{o}C. At this temperature, S^{2-} ions are released by the alkaline hydrolysis of thiourea and reacted with Cd^{2+} yielding CdS nanocrystals. After 1 hour of heating, a yellow transparent solution was formed indicative of the formation of the CdS-TND hybrids. To this clear solution acetone was added in excess to precipitate CdS-TNDs. The yellow precipitate was then washed several times with acetone and finally re-dispersed in water for a subsequent CdS growth cycle. To start the second CdS growth cycle, the CdS-TND hybrids obtained in the previous cycle was used as precursor instead of TEA-TNDs. The following steps were similar to those of the previous cycle. This CdS growth cycle was repeated 5 times to obtain the final TND-CdS hybrid colloids. The obtained CdS-TND hybrids were dispersed in water with the concentration of 10 mg/cm^3.

Synthesis of CdS-TND-Ni nanocomposites. To the CdS-TND hybrid solution was added a solution of $Ni(NO_3)_2$ (Ni^{2+}:Ti molar ratio of 1:20). The mixture was then stirred for 1 hour. During this process, Ni^{2+} was adsorbed on the surface of TNDs through cation exchange process with TEA^+, resulting in CdS-TND-Ni^{2+}. The obtained CdS-TND-Ni^2 was then precipitated from the solution by adding an excess amount of acetone to remove any possible non-exchanged Ni^{2+}. The obtained precipitate was washed with acetone to remove the physically adsorbed Ni^{2+} on the CdS surface to ensure that Ni^{2+} only appeared on the surface of TNDs before being reduced. The CdS-TND-Ni^{2+} was then re-dispersed in an aqueous ethanol solution 20% (v/v) in a gas-tight reaction cell. The solution was evacuated and purged with nitrogen for 10 minutes to completely remove the dissolved oxygen. Finally, the solution was illuminated for 2 hours by a 300W Xe arc lamp equipped with an UV-cutoff filter (≥420 nm). The obtained CdS-TND-Ni NC solution was kept under nitrogen for photocatalytic hydrogen generation test.

Synthesis of CdS nanoparticles. Pure CdS nanoparticles were prepared in the similar conditions to those of the CdS-TND hybrids, but in the absence of TNDs. A mixture of TEAOH and thiourea was added to the solution containing Cd^{2+} cations. The mixture was then heated to 70°C for 1 hour. The resulting precipitate was then washed several times with water and dried at 70°C for 5 hours.

Characterization. Transmission electron microscopy (TEM) images of the samples were obtained on a JOEL JEM 1230 operated at 120kV. High resolution TEM (HRTEM) images were performed on Philips G2 F30 Tecnai instrument operated at 300kV. Powder X-ray diffraction (XRD) patterns of the samples were obtained on a Bruker SMART APEXII X-ray diffractometer equipped with a Cu Kα radiation source (λ=1.5418 Å). Thermal analyses of the samples were carried out at a heating rate of 10 °C/min under a nitrogen flow up to 700 °C using a Perkin-Elmer TGA thermogravimetric analyzer. Zeta potential measurements were performed with a Zetasizer Nano ZS in water at 25 ^{o}C. X-ray photoelectron spectroscopy (XPS) measurements carried out in an ion-pumped chamber (evacuated to 10-9 Torr) of a photoelectron spectrometer (Kratos Axis-Ultra) equipped with a focused X-ray source (Al Kα, hv = 1486.6 eV). The UV-vis spectra were recorded on a Cary 300 Bio UV-visible spectrophotometer. Fourier transform infrared (FTIR) absorption spectra were measured with a FTS 45 infrared spectrophotometer with the KBr pellet technique.

Photocatalytic testing.

Photocatalytic reactions for hydrogen production under natural sunlight were carried out in an air-tight Pyrex tube reactor (irradiation area of 125 cm^2). Photocatalyst samples (0.1 g) were dispersed in 500 mL of an ethanol-water mixture (20 v/v %) in the reactor. The solution was purged with N_2 gas for 30 min before reaction in order to eliminate dissolved oxygen. The volume of gas produced was measured by recording the displacement of water level in an inverted and graduated water-filled burette. The hydrogen gas produced was also confirmed by gas chromatography equipped with TCD detector and carboxen-1010 capillary column.

The photocatalytic hydrogen generation experiments were also performed under visible light irradiation for the purpose of comparison between the samples. The photocatalytic reactions were carried out in a gas-tight 200 ml Pyrex reaction cell at ambient temperature and atmospheric pressure under visible light illumination. In a typical photocatalytic experiment, 20

mg of photocatalysts were dispersed in 70 ml of aqueous solution containing 20 % (v/v) of ethanol. In the case of CdS-Ni and CdS-Pt photocatalyts, $Ni(NO_3)_2$ and H_2PtCl_6 (1.2 wt% of metallic cocatalysts) were also added, respectively. The mixture was evacuated and purged with nitrogen for 30 minutes to remove dissolved oxygen. Then, it was illuminated with a 300W Xe arc lamp equipped with an UV-cutoff filter (≥420 nm) under stirring condition. A 0.5 mL of gas was sampled intermittently through the septum, and hydrogen was analyzed by gas chromatography equipped with TCD detector and carboxen-1010 capillary column.

The apparent quantum yield (QY) was measured under the same photocatalytic reaction conditions. The photon flux was measured with Newport's power meter equipped with a thermopile optical detector.

. The QY was calculated according to following equation:

$$QY\ (\%) = \frac{\text{Number of reacted electron}}{\text{Number of incident photons}} \times 100$$

$$= \frac{\text{Number of evoled } H_2 \text{ molecules } \times\ 2}{\text{Number of incident photons}} \times 100$$

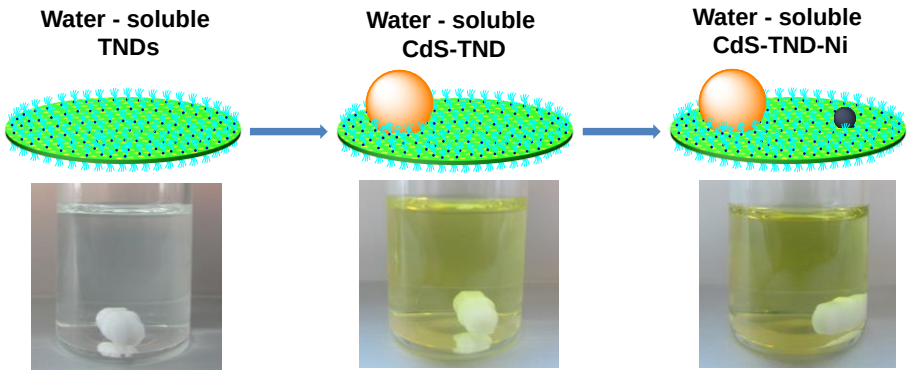

Scheme S1. Schematic illustration of the three steps in the preparation of water-soluble CdS-TND-Ni NCs: (i) synthesis of water-soluble TNDs; (ii) assembly of CdS-TND hybrids; and (iii) formation of water-soluble CdS-TND-Ni NCs.

Table S1. H_2 production rates of reported related CdS based photocatalysts with or without using noble metal cocatalysts

	Photocatalysts	Light source	Sacrificial agent	H_2 generation rate (mmol. h^{-1}. g^{-1})	Refs
Without noble metal cocatalysts	CdS-NiS	Xe-arc 300W, λ≥420 nm	Na_2S + Na_2SO_3	~ 0.600	1
	CdS-$Ni(OH)_2$	Xe-arc 300W, λ≥420 nm	Ethanol	1.461	2
	CdS-$Ni(OH)_2$	Xe-arc 300W, λ≥420 nm	Na_2S + Na_2SO_3	1.556	2
	CdS-NiO	Halogen 500W	Na_2S + Na_2SO_3	0.745	3
	CdS-MoS_2	Xe-arc 300W, λ≥420 nm	Ethanol	~ 0.240	4
	CdS-$KNbO_3$-NiO_x	Hg-Xe 500W, λ≥400 nm	isopropanol	0.150	5
	CdS-Graphene	Xe-arc 200W, λ≥420 nm	Na_2S + Na_2SO_3	0.700	6
	CdS-(N-graphene)	Xe-arc 300W, λ≥420 nm	Na_2S + Na_2SO_3	1.050	7
	CdS-titanate nanosheet	Xe-arc 300W, λ≥420 nm	Na_2S + Na_2SO_3	1.020	8
	CdS-titanate	Xe-arc 800W, λ≥420 nm	Na_2S + Na_2SO_3	~ 0.075	9
	CdS-carbon nanotube	Xe-arc 300W, λ≥400 nm	Na_2S + Na_2SO_3	0.092	10
	CdS-titanate nanotube	Xe-arc 500W, λ≥420 nm	Na_2S + Na_2SO_3	~ 0.450	11
	Water-soluble CdS-TND-Ni	**Xe-arc 300W, λ≥420 nm**	**Ethanol**	**11.038**	This work
	Water-soluble CdS-TND-Ni	**Natural sunlight**	**Ethanol**	**31.820**	This work
With noble metal cocatalysts	CdS-TiO_2-Pt	Hg-arc 500W, λ≥420 nm	Na_2S + Na_2SO_3	~4.00	12
	CdS-ZnO-Pt	Xe-arc 300W	Na_2S + Na_2SO_3	3.870	13
	CdS-(g-C_3N_4)-Pt	Xe-arc 300W, λ≥400 nm	Methanol	0.173	14
	(c-CdS)-Pt-(hex-CdS)	Hg – Xe, λ≥400 nm	isopropanol	0.153	15
	(c-CdS)-Pt-(hex-CdS)	Hg – Xe, λ≥400 nm	Na_2S + Na_2SO_3 + NaOH	0.668	15
	CdS-graphene oxide-Pt	Hg 400W, λ = 365 nm	Methanol	5.500	16
	CdS-titanate nanotube-Pt	Xe-arc 500W, λ≥420 nm	Na_2S + Na_2SO_3	~ 1.750	11
	CdS-carbon nanotube-Pt	Xe-arc 300W, λ≥400 nm	Na_2S + Na_2SO_3	0.819	10
	CdS-ZnO-Au	Xe-arc 300 W	Na_2S + Na_2SO_3	0.608	17
	CdS:Mn-RuO_x	Xe-arc 500W, λ≥420 nm	Na_2S + Na_2SO_3	1.935	18
	ZnO-CdS@Cd-Pt	Xe-arc 300 W	Na_2S + Na_2SO_3	19.200	19

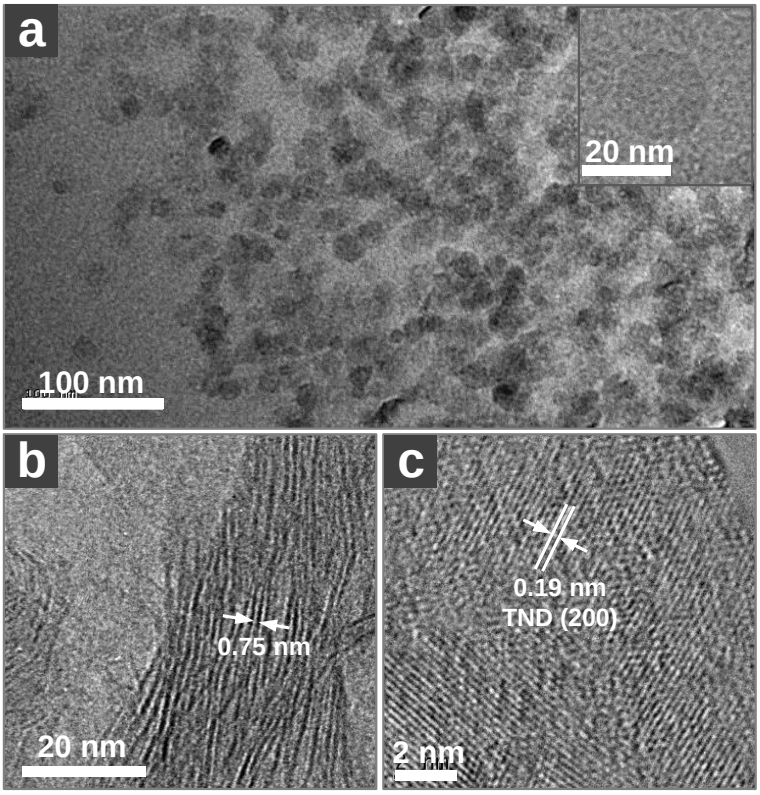

Figure S1. TEM images of the as-synthesized TNDs dispersed in toluene (a), and precipitated in ethanol (b), and HRTEM of TNDs aligned perpendicular to the electron beam (c). Due to the ultrathin structure of TNDs, in the highly dispersed state (i.e. dispersed in toluene), these TNDs tend to lay parallel to the surface of the TEM's grid. Thus, a mean TND's diameter of around 20 nm can be observed (figure a). In the precipitated state (i.e. precipitated in ethanol), some aggregate of TNDs could lay parallel to the direction of the electron beam (figure b), we therefore can calculate the thickness of the TNDs (0.75 nm). Figure c shows a d-spacing of 0.19 nm which is corresponding to the crystalline lattice of (200) plane in the lepidocrocide-type titanate structure.

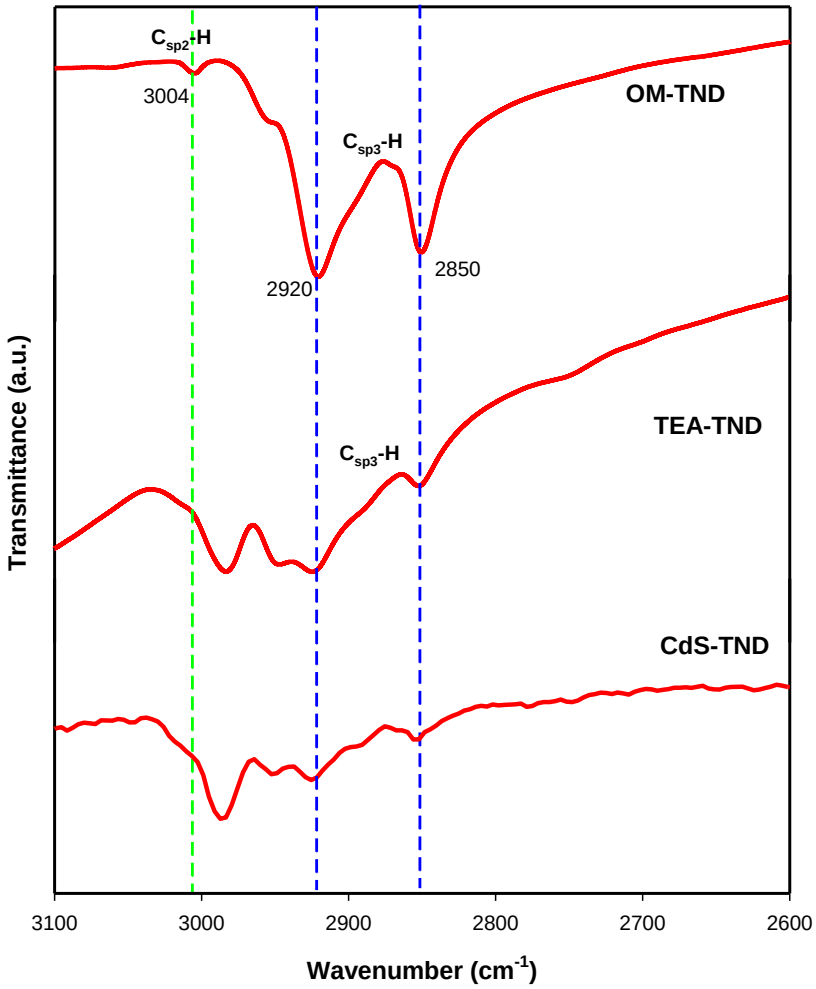

Figure S2. FTIR spectra of as-synthesized OM-TND, TEA-TND obtained by treated OM-TND with TEA, and CdS-TND hybrids. FTIR spectra of all samples show two peaks at 2920 and 2850 cm^{-1} corresponding to the asymmetric and symmetric stretching mode of methylene groups present in the alkyl chain of OM and TEA, respectively. In addition, no absorption at 3004 cm^{-1} which would correspond to the stretching vibration of the C-H bond in the C=C group of OM molecules presents on the FTIR spectrum TEA-TND, indicating that the OM molecules adsorbed on the surface of TNDs have been fully displaced by the TEA cations.

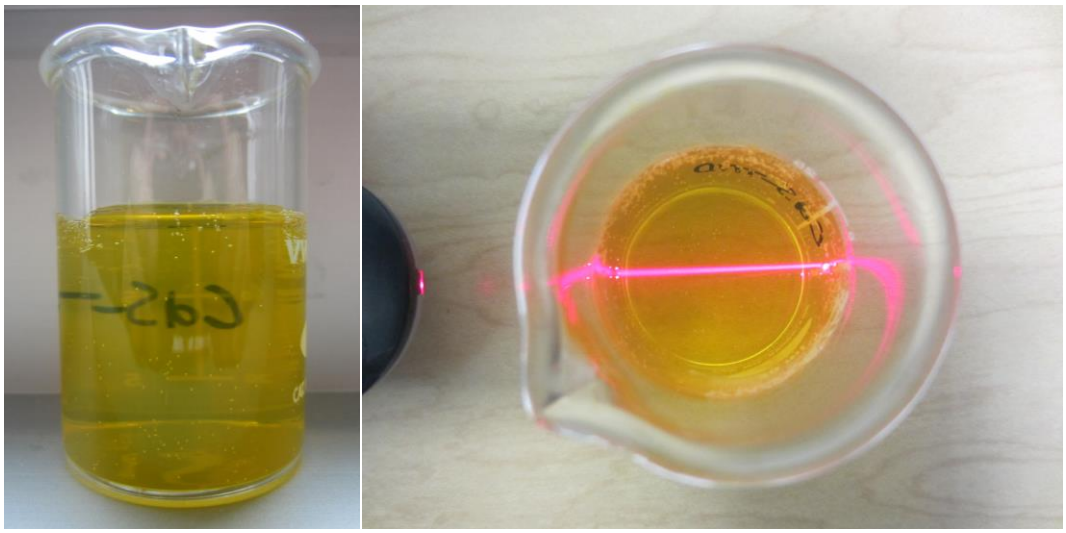

Figure S3. Photo of CdS-TND hybrid colloidal solution showing a clear transparency (left). Photo of CdS-TND solution with a typical Tyndall Effect of colloidal solution.

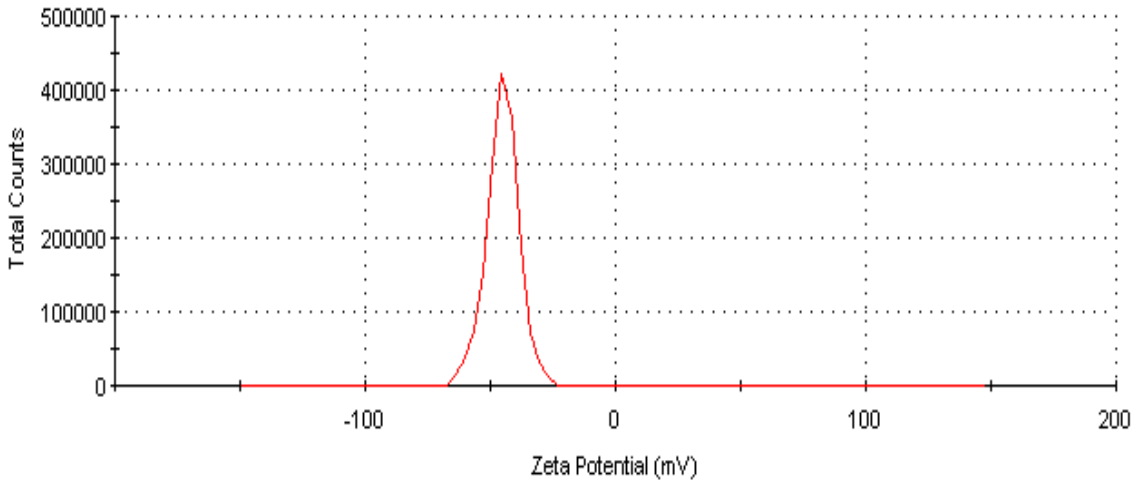

Figure S4. Zeta potential of CdS-TND hybrid colloidal solution measured at pH = 7.5. The CdS-TND solution exhibited a negative zeta potential of 46 mV, indicating a high stability of this colloidal solution. ASTM defines colloids with zeta potentials higher than 40 mV (negative or positive) to have "good stability." [20]

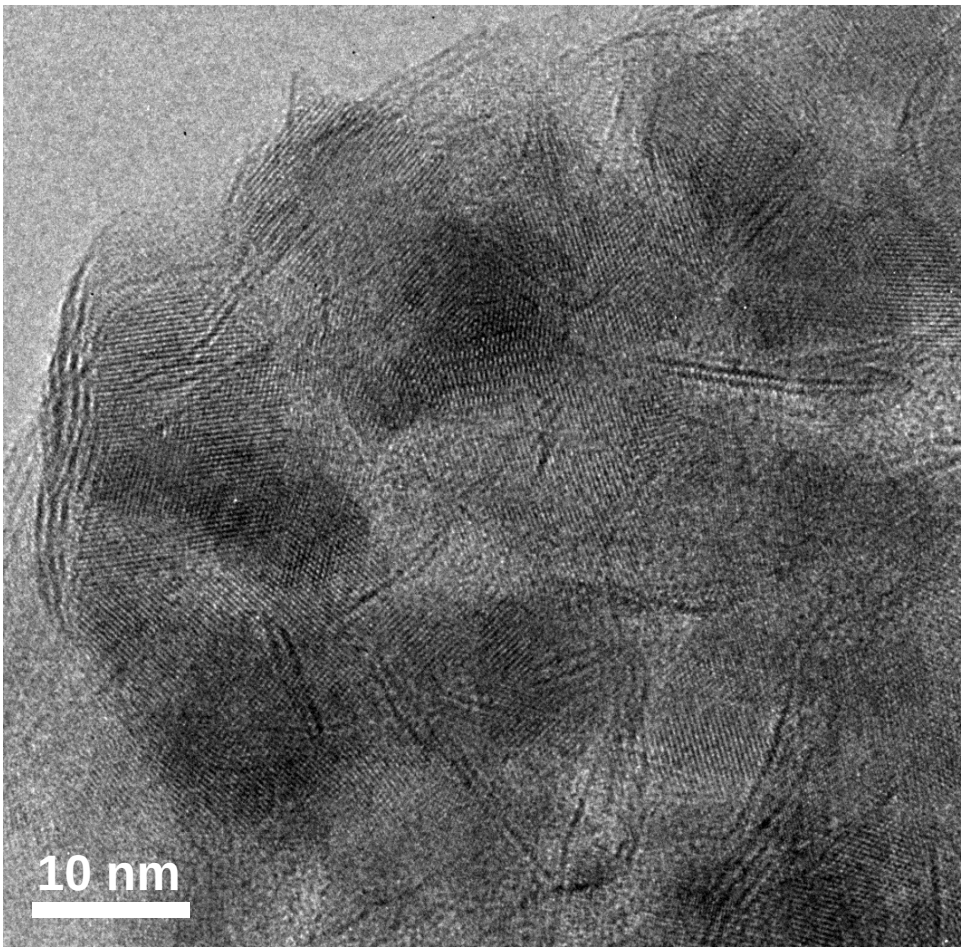

Figure S5. Large area HRTEM image of CdS-TND hybrid obtained by 5 cycles of CdS growth showing the intimate contact between CdS nanoparticles and TNDs

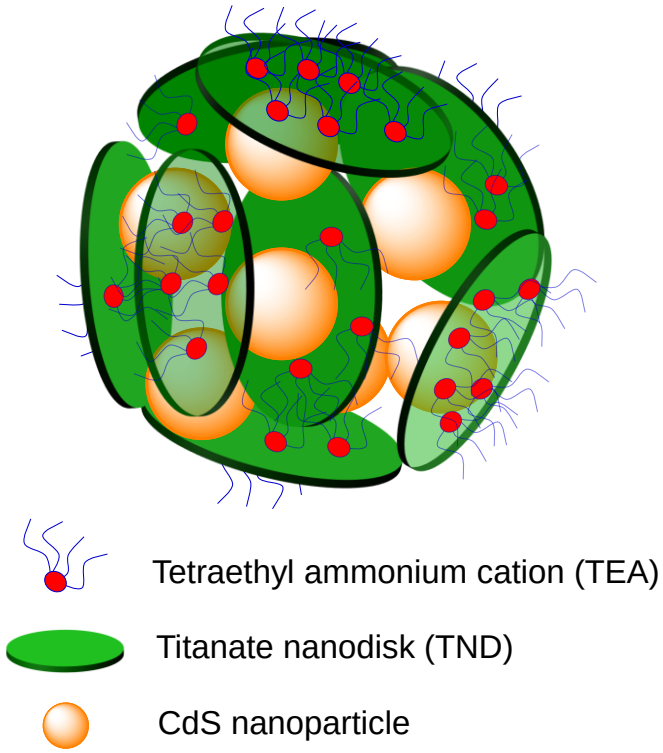

Figure S6. Schematic illustration of the structure of CdS-TND hybrid colloid. Each colloid consists of several TNDs and CdS nanoparticles. The TNDs and CdS nanoparticles are mutually intercalated forming hybrid colloids with multipoint contacts at the interface between the two nano-domains.

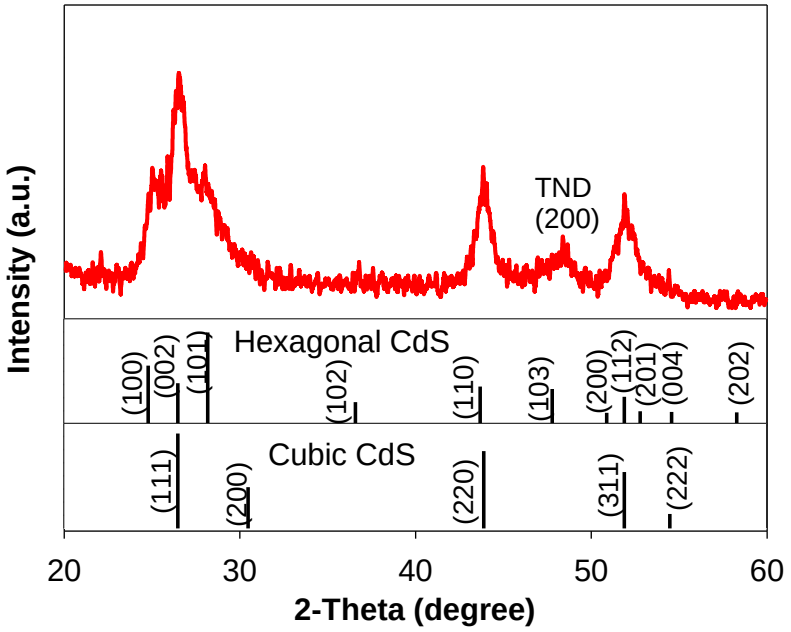

Figure S7. Wide angle powder XRD pattern of the CdS-TND hybrid obtained upon 5 cycles of CdS growth. The standard XRD patterns of cubic and hexagonal CdS are also provided.

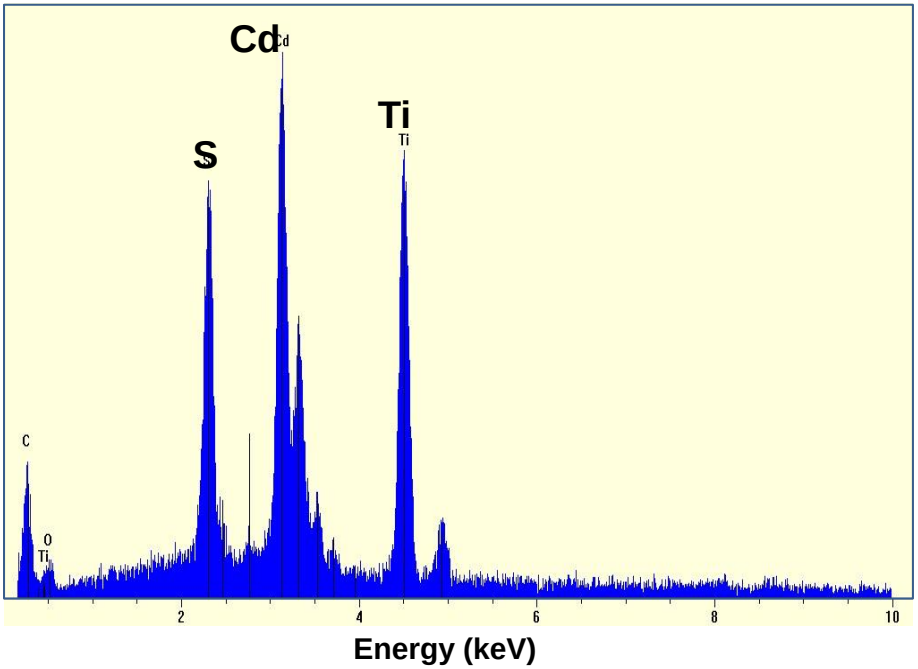

Figure S8. EDX spectrum of CdS-TND hybrids obtained by 5 cycles of CdS growth showing a Cd:Ti molar ratio of 1.14:1.

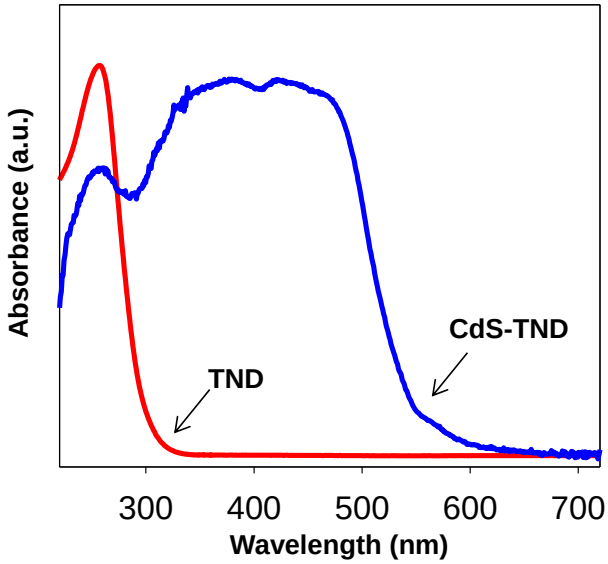

Figure S9. UV-vis diffusive reflectance spectra of the CdS-TND hybrids in comparison to that of TNDs.

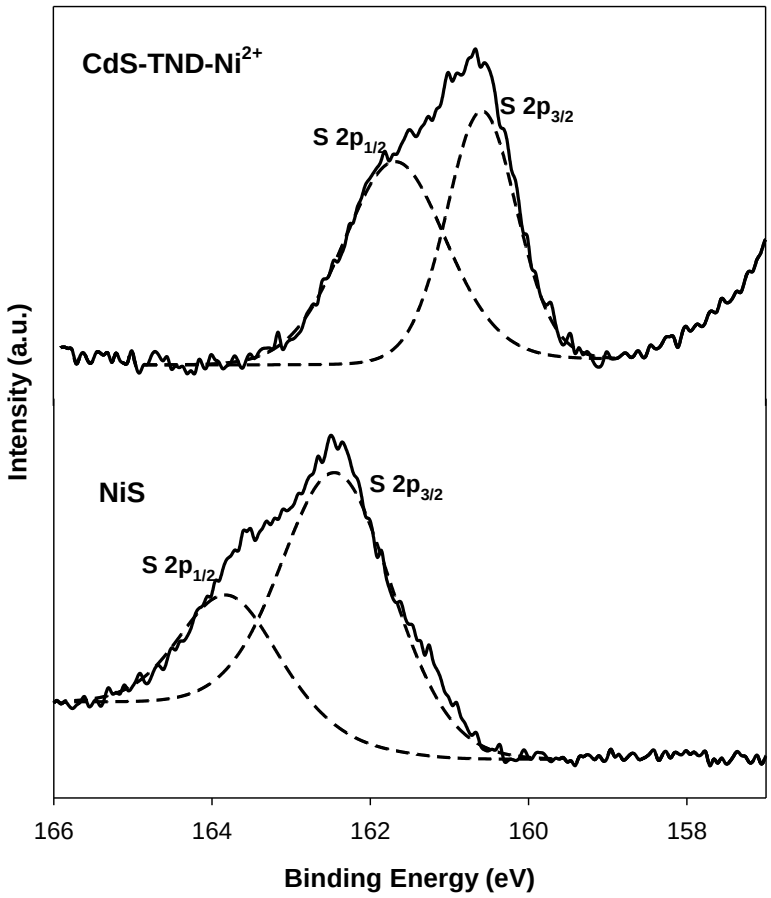

Figure S10. XPS spectrum of S 2p in the CdS-TND-Ni^{2+} in comparison to that of S 2p in NiS prepared by reacting Ni^{2+} with Na_2S. It is observed that, the S 2p XPS spectrum of CdS-TND-Ni^{2+} shows two peaks at 160.5 and 161.6 eV, corresponding to the binding energy of S $2p_{3//2}$ and S $2p_{1/2}$, respectively.[21] No peaks at 162.3 and 163.7 eV in the S 2p XPS spectrum of NiS[22] was observed in the S 2p XPS spectrum of CdS-TND-Ni^{2+}, indicating the absence of NiS in the CdS-TND-Ni^{2+}.

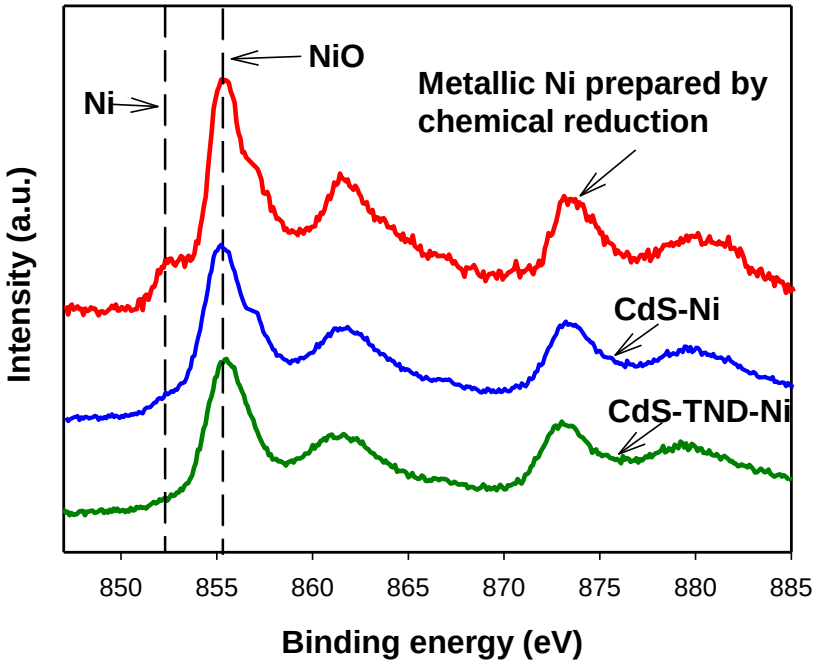

Figure S11. XPS spectrum of Ni 2p in the CdS-TND-Ni NCs in comparison to those of Ni in CdS-Ni obtained by photoreduction of Ni^{2+} on CdS, and metallic Ni nanoparticles prepared by chemical reduction using $NaBH_4$ as reducing agent and $Ni(NO_3)_2$ as nickel precursor.

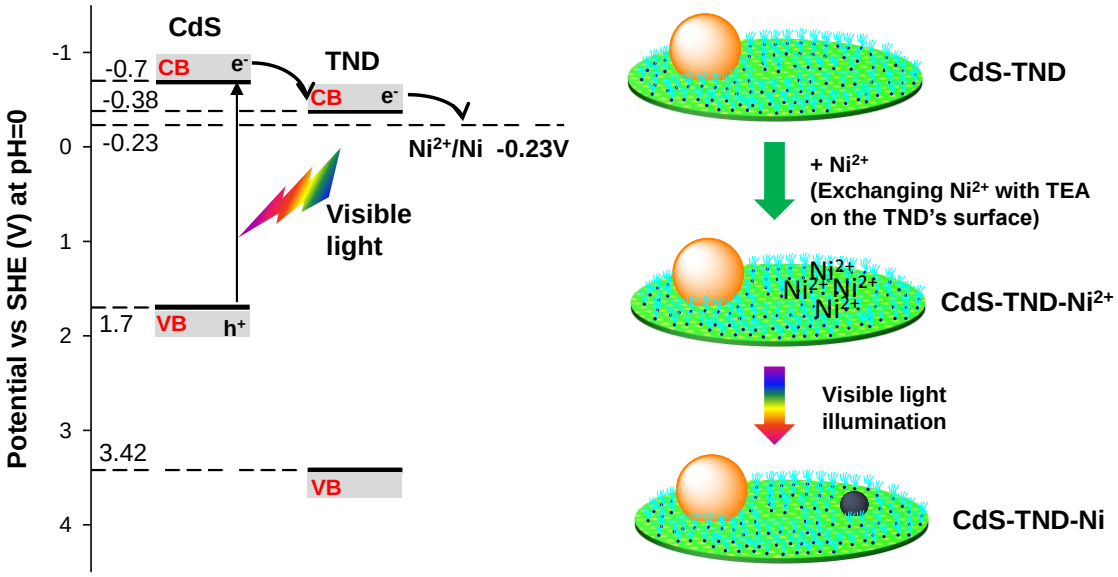

Figure S12. Schematic illustration of the electron transfer in the photoreduction of Ni^{2+} adsorbed on the surface of TNDs under visible light illumination (left). Schematic illustration of the formation of Ni clusters on the surface of TND in the CdS-TND hybrids by visible light illumination (right).

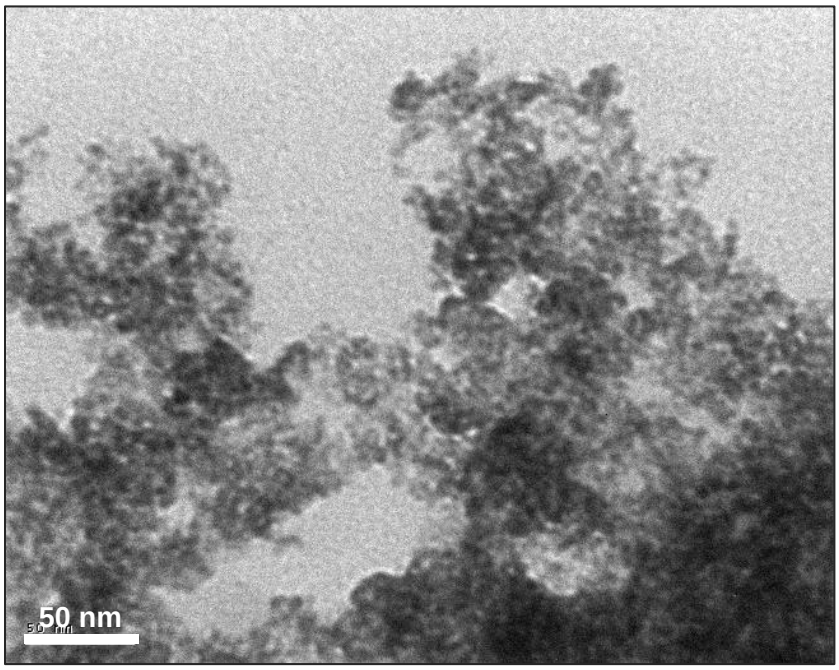

Figure S13. TEM image of CdS nanoparticles obtained under similar conditions to those of CdS-TND hybrids, except for the absence of TNDs. It can be seen that, the size of the CdS nanoparticles are around 6 nm which are similar to those of CdS nanoparticles in the CdS-TND-Ni nanocomposites. These CdS nanoparticles are aggregated forming large precipitate.

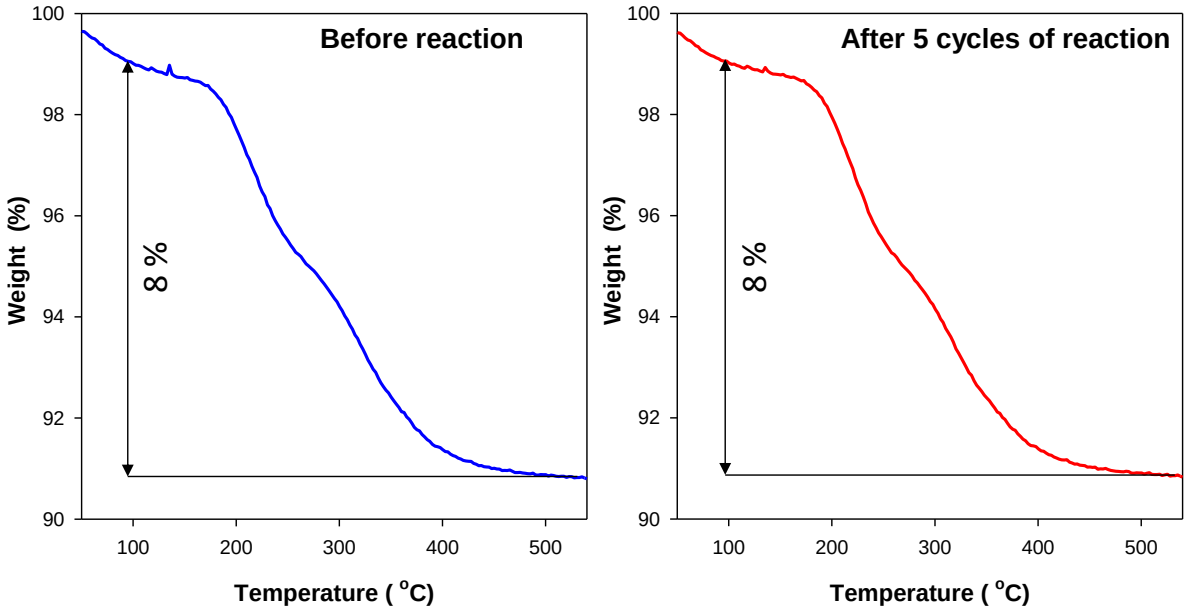

Figure S14. TGA curves of CdS-TND-Ni NCs before and after 5 cycles of hydrogen generation reaction.

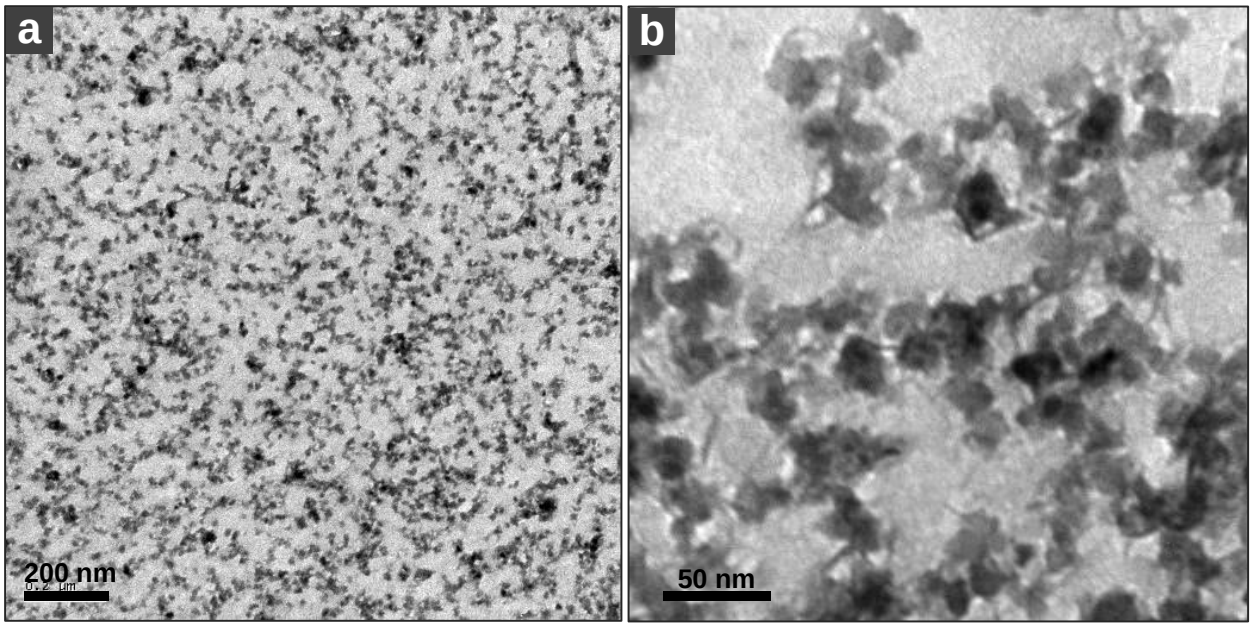

Figure S15. Low magnification (a) and high magnification (b) TEM images of CdS-TND-Ni nanocomposites after 5 cycles (15 h) of reaction. The low magnification image shows that the photocatalysts are still highly dispersed in solution after the reaction. The high magnification image reveals that the morphology of the CdS-TND-Ni nanocomposites is preserved after 5 cycles.

References

1. Chen, X.; Chen, W.; Lin, P.; Yang, Y.; Gao, H.; Yuan, J.; Shangguan, W. *Catal. Commun.* **2013**, *36*, 104.
2. Ran, J.; Yu, Y. G.; Jaroniec, M. *Green Chem.* **2011**, *13*, 2708.
3. Khan, Z.; Khannam, M.; Vinothkumar, N.; De, M.; Qureshi, O. *J. Mater. Chem.* **2012**, *22*, 12090.
4. Zong, X.; Wu, G.; Yan, H.; Ma, G.; Shi, J.; Wen, F.; Wang, L.; Li, C. *J. Phys. Chem. C* **2010**, *114*, 1963.
5. Choi, J.; Ryu, S. Y.; Balcerski, W.; Lee, T. K.; Hoffmann, M. R. *J. Mater. Chem.* **2008**, *18*, 2371.
6. Ye, A.; Fan, W.; Zhang, Q.; Deng, W.; Wang, Y. *Catal. Sci. Technol.* **2012**, *2*, 969.
7. Jia, L.; Wang, D. H.; Huang, Y. X.; Xu, A. W.; Yu, H. Q. *J. Phys. Chem. C* **2011**, *115*, 11466.
8. Kim, H. N.; Kim, T. W.; Kim, I. Y.; Hwang, S. J. *Adv. Funct. Mater.* **2011**, *21*, 3111.
9. Zhang, Y.; Tang, Y.; Liu, X.; Dong, Z.; Hng, H. H.; Chen, Z.; Sum, T. C.; Chen, X. *Small* **2013**, *9*, 996.
10. Kim, Y. K.; Park, H. *Energy Environ. Sci.* **2011**, *4*, 685.
11. Chen, Y.; Wang, L.; Lu, G. M.; Yao, X.; Guo, L. *J. Mater. Chem.* **2011**, *21*, 5134.
12. Jang, J. S.; Choi, S. H.; Kim, H. G.; Lee, J. S. *J. Phys. Chem. C* **2008**, *112*, 17200.
13. Wang, X.; Liu, G.; Chen, Z. G.; Li, F.; Wang, L.; Lu, G. Q.; Cheng, H. M. *Chem. Commun.* **2009**, 3452.
14. Ge, L.; Zuo, F.; Liu, J.; Ma, Q.; Wang, C.; Sun, D.; Bartels, L.; Feng, P. *J. Phys. Chem. C* **2012**, *116*, 13708.
15. Silva, L. A.; Ryu, S. Y.; Choi, J.; Choi, W.; Hoffmann, M. R. *J. Phys. Chem. C* **2008**, *112*, 12069.
16. Gao, P.; Liu, J.; Lee, S.; Zhang, T.; Sun, D. D. *J. Mater. Chem.* **2012**, *22*, 2292.
17. Yu, Z. B.; Xie, Y. P.; Liu, G.; Lu, G. Q. M.; Ma, X. L.; Cheng, H. M. *J. Mater. Chem. A*, **2013**, *1*, 2773.
18. Ikeue, K.; Shiiba, S.; Machida, M. *Chem. Mater.* **2010**, *22*, 743.
19. Wang, X.; Liu, G.; Wang, L.; Chen, Z. G.; Lu, G, Q, M.; Cheng, H. M. *Adv. Energy Mater.* **2012**, *2*, 42.

20. *Zeta Potential of Colloids in Water and Waste Water*, ASTM Standard D 4187 - 82, American Society for Testing and Materials, 1985.
21. Bhide, V.G.; Salkalachen, S.; Rastog, A.C.; Rao, C.N.R.; Hegde, M.S. *J. Phys. D: Appl. Phys.* **1981**, *14*, 1647.
22. Shalvoy, R.B.; Reucroft, P.J. *J. Vac. Sci. Technol.* **1979**, *16*, 567.